Design of IPM Synchronous Machines Using Fast-FEA Corrected Design Equations

Terms of use:

(Article begins on next page)

01 September 2025

Design of IPM Synchronous Machines Using Fast-FEA Corrected Design Equations

Paolo Ragazzo, *Student Member, IEEE*, Gaetano Dilevrano, *Student Member, IEEE*
Simone Ferrari, *Member, IEEE* and Gianmario Pellegrino, *Fellow, IEEE*

Abstract—This paper proposes a procedure for the fast preliminary design of Internal Permanent Magnet machines for traction application. Given the stack diameter and electric loading, the method permits to quickly determine the rotor diameter, stator slots and rotor cavities dimensions, and the stack length using FEA-corrected design equations, without time-consuming optimization. The core of the proposed method is the torque and power factor design plane function of the (x, b) coordinates, the former being the rotor to stator diameter ratio and the latter the p.u. iron size. The torque and power factor equations versus (x, b) are formulated using the magnetic equivalent circuit of the machine and then refined via a few selected FEA simulations. A comprehensive design procedure is built, using the Tesla Model 3 motor ratings as reference with a focus on key design inputs as the current and voltage limits and the feasible numbers of turns.

Index Terms—AC motors, design methodology, finite element methods, synchronous permanent magnet machines, V-shape IPM, electric traction motors.

I. INTRODUCTION

Internal Permanent Magnet (IPM) machines are a competitive solution in many fields of applications, ranging from vehicular traction [1] to aviation [2], [3] to wind power generation [4], [5]. The high cost of Permanent Magnet (PM) materials [6] pushes the automotive industry towards the maximization of the reluctance torque contribution and the corresponding minimization of the PM quantity [1]. Nevertheless, IPM machines based on rare-earth magnets remain the state of the art solution for traction.

The literature proposes several approaches for the design of IPM machines. Those based on purely analytical models [7], [8] are known for poor accuracy. Most of to date methods rely on Finite Element Analysis (FEA) and massive use of algorithmic optimization [9], [10], which is also called the brute force approach for its high computational burden and limited insight of the designer [11]. A hybrid FEA and equations approach was proposed in [7] and [12] for the design of Synchronous Reluctance (SyR) machines.

This paper extends the fast FEA refinement (FEAfix) procedure of [7] to the design of IPM machines with V-type rotors. Note that respect to [7], the axes convention is changed: what was the d-axis is here q-axis, as the

P. Ragazzo, G. Dilevrano, S. Ferrari and G. Pellegrino are with the Department of Energy "Galileo Ferraris" Politecnico di Torino, 10129 Turin, Italy (e-mail: paolo.ragazzo@polito.it gaetano.dilevrano@polito.it simone.ferrari@polito.it gianmario.pellegrino@polito.it).

Fig. 1 highlights. The PMs are included into the design equations and FEAfix corrected for accounting for the exact Maximum Torque per Ampere (MTPA) operating condition. The paper shows how the design plane can be powerfully used to cross match the key design requirements of peak torque and power, given the stack dimensions with the power converter voltage and current limits. Moreover, axial length minimization and PM mass minimization are quantitatively studied starting from graphical representations on the design plane then confirmed by FEA results. Also, another critical conflict addressed in the paper is between electromagnetic performance and structural integrity [13]. Here, the ribs are analytically sized, representing a good starting point for more detailed mechanical optimization.

The proposed design process applies to the design of V-shape IPM traction motors and the term of comparison used in the paper is the Tesla Model 3 IPM motor, which main specifications are summarized in Table I.

The FEA model of the benchmark case is reported in Fig. 1, as reconstructed by various literature sources such as [14]. The proposed method is integrated in the open-source design and simulation platform SyR-e [15].
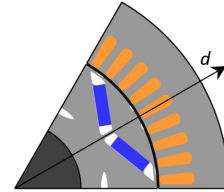

Fig. 1: Cross-section of the Tesla Model 3 IPM motor.

TABLE I: Tesla Model 3 requirements

Max current	I_{max}	<1414	[Apk]
Max current density	J_{max}	<36	[Apk/mm^2]
Max torque	T_{max}	>430	[Nm]
Min DC link voltage	V_{dc}	<231	[V]
Base speed	n_{base}	>4200	[rpm]
Max speed	n_{max}	>18100	[rpm]
Max power	P_{max}	>192	[kW]
Stator diameter	D	<225	[mm]
Airgap	g	0.7	[mm]
Stack length	L	<132	[mm]
PM weight	m_{pm}	<1.8	[kg]

II. DESIGN EQUATIONS AND DESIGN PLANE

A. Torque and Power Factor (x, b) Design Plane

The peak torque at maximum inverter current and the peak power at maximum converter current and voltage requirements of the application are considered for the magnetic design of the machine and the definition of the stator and rotor geometry. Same as in [7], the torque and power factor (PF) plane is considered, function of the geometric input parameters x and b (1).

$$x = \frac{D_r}{D} \qquad b = \frac{B_g}{B_{Fe,s}} \tag{1}$$

Where x is the ratio between the rotor diameter (D_r) and the stator diameter (D), and b is the ratio between the airgap peak and back-iron iron peak flux density values, summarizing the size of the iron flux paths with respect to the size of non-iron paths such as the stator slots and the PM pockets in the rotor.

The peak power specification is translated into the target base speed (2) and therefore the target PF at base speed (3) at peak torque and current conditions, considering the dc-link voltage V_{dc}:

$$n_{base} = \frac{30}{\pi} \cdot \frac{P_{max}}{T_{max}} \geq 4200 rpm \tag{2}$$

$$(cos\varphi)_{base} = \frac{2}{\sqrt{3}} \frac{P_{max}}{V_{dc} \cdot I_{max} \cdot \eta} \approx 0.71 \tag{3}$$

The efficiency in (3) is conservatively assumed as $\eta = 0.95$. Both base-speed and PF equations refer to MTPA conditions.

The area of feasible designs in the (x, b) plane is where $T(x, b) \geq T_{max} = 430$ Nm and $PF(x, b) \geq (cos\varphi)_{base} = 0.71$. If both conditions are met, also the peak power condition is met.

B. Torque and Power Factor Equations

The dq-flux linkage versus current equations of the IPM machine are reported in (4), with the d-axis direction defined in Fig. 1.

$$\begin{cases} \lambda_d = (L_{md} + L_\sigma) \cdot i_d + \lambda_m \\ \lambda_q = (L_{mq} + L_\sigma) \cdot i_q \end{cases} \tag{4}$$

The equations give evidence of the four parameters L_{md}, L_{mq} (magnetizing inductance), L_σ (leakage inductance) and λ_m (magnet flux linkage) that will be analytically evaluated. The familiar dq inductance values are $L_d = L_{md} + L_\sigma$ and $L_q = L_{mq} + L_\sigma$. The torque equation, with evidence of the said parameters, is (5).

$$T = \frac{3}{2} p \left[\lambda_m \cdot i_q + (L_{md} - L_{mq}) \, i_d i_q \right] \tag{5}$$

where p is the number of pole pairs. Neglecting the stator resistance voltage, the PF is expressed as:

$$cos\varphi = sin(\gamma - \delta) \tag{6}$$

where γ is the current phase angle and δ is the flux phase angle with respect to the d-axis. Torque. As said, the PF will be evaluated at MTPA conditions.
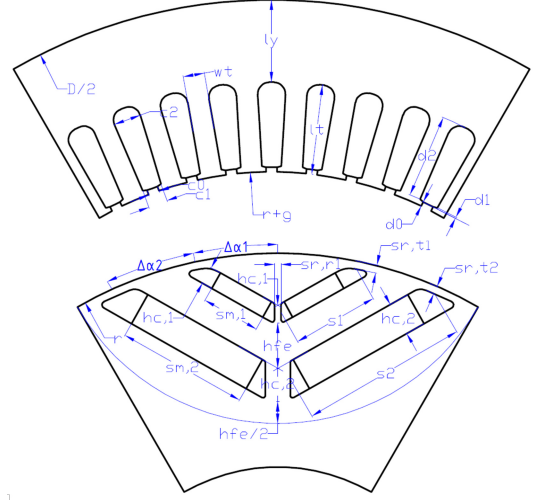
C. q-axis Design: Stator and Rotor Iron Size

Fig. 2: V-shaped stator and rotor parameters.

The q-axis design rules define the dimensions of the stator back iron and teeth and the size of the rotor flux carriers given the input (x, b). The geometric parameters are defined in Fig. 2. The stator yoke size l_y is determined as (7).

$$l_y = \frac{D}{2p} \cdot k_y \cdot xb \tag{7}$$

The reference condition $k_y = 1$ for the non-dimensional yoke-length factor refers to the case of a sinusoidal airgap flux density of amplitude B_g turning into a back-iron flux density of $B_{Fe,s} = \frac{B_g}{g}$. The tooth size is defined by the equation (8)

$$w_t = \frac{\pi D}{6pq} \cdot x \cdot b \cdot k_t \tag{8}$$

where the tooth width factor $k_t = \frac{B_{Fe,s}}{B_{tooth}}$ defines the tooth size with respect to the yoke size. A value $k_t < 1$ is normally selected, standing for the tooth more saturated than the back-iron [16].

Dealing with the size of rotor iron paths, the default design condition is that the sum of the flux carriers size ($l_r = h_{Fe} + h_{Fe}/2$ as defined in Fig. 2) equals the stator back iron size l_y. In (9), the rotor carrier thickness factor $k_{Fe,r}$ is introduced to vary the rotor carriers size with respect to the default condition. In this case study, a value of $k_{Fe,r} = 1.1$ is chosen.

$$k_{Fe,r} = \frac{l_r}{l_y} \tag{9}$$

The i_q current Ampere-turns are evaluated to impose the target airgap flux density. Neglecting the PM contribution,

equation (10) is obtained by the Ampere's law with ideal iron.

$$N_s i_q = \frac{\pi}{3} \frac{k_c g}{\mu_0} \frac{p}{k_w} \cdot B_{Fe} \cdot b \qquad (10)$$

Where N_s is the number of turns in series per phase and k_w is the winding factor. Saturation of the q-axis magnetic path is accounted for through a saturation coefficient $k_{sat} \geq 1$ is adopted, as defined in [7].

D. d-axis design: rotor barriers and PMs

The magnetic circuit model accounting for the d-axis MMF and related flux components is represented in Fig. 3. The circuit represents half a pole of the machine in the general case of n flux barriers.

The stator MMF excited by the i_d Ampere-turns is represented by the ΔF_s generators in the circuit, according to the staircase model defined in [7]. The j-th MMF step derives from $N_s i_d$ according to (11).

$$\Delta F_{sj} = \frac{3}{\pi} \frac{N_s i_d}{p} k_w \cdot k_{stair,j} \qquad (11)$$

Where $k_{stair,j}$ defines the step amplitude, with reference to the per-unit MMF staircase [7]. The d current component is calculated by vector difference between I_{max} and i_q.

Under the assumption of rotor regular pitch, the airgap reluctance $\mathfrak{R}_g$ is

$$\mathfrak{R}_g = \frac{2g \cdot k_c}{\mu_0 \cdot \alpha \cdot x \cdot DL} \qquad (12)$$

where g is the airgap length, k_c is the Carter coefficient, α is the airgap angular pitch between two adjacent barriers and L is the stack length.

Looking into the magnetic circuit of one barrier (Fig. 4), this accounts for a PM branch ($\mathfrak{R}_m$ and ϕ_m), an air branch ($\mathfrak{R}_a$) accounting for the portion of barrier not filled
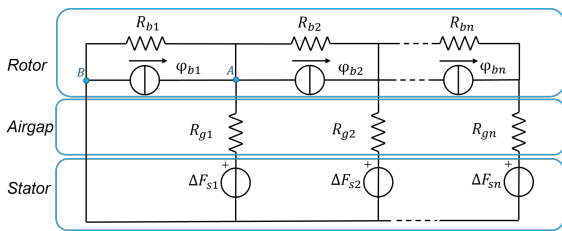

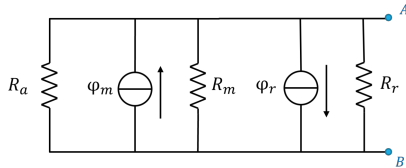Fig. 3: Magnetic circuit of a PM Synchronous machine with n barriers rotor.

Fig. 4: Equivalent circuit of one rotor barrier.

with magnet, and a ribs branch ($\mathfrak{R}_r$ and ϕ_r). The respective reluctances are obtained as:

$$\mathfrak{R}_a = \frac{h_a}{\mu_0 s_a L} \quad , \quad \mathfrak{R}_m = \frac{h_m}{\mu_0 \mu_m s_m L} \qquad (13, 14)$$

$$\mathfrak{R}_r = \frac{h_r}{\mu_0 \mu_r (s_{r,t} + s_{r,r}/2) \cdot L} = \frac{h_r}{\mu_0 \mu_r s_r L} \qquad (15)$$

The Norton equivalent at the AB nodes is obtained with (16) and (17).

$$\mathfrak{R}_b = \left(\frac{1}{\mathfrak{R}_a} + \frac{1}{\mathfrak{R}_m} + \frac{1}{\mathfrak{R}_r} \right)^{-1}, \quad \varphi_b = \varphi_m - \varphi_r \quad (16, 17)$$

The magnet flux φ_m and the absorbed total ribs flux φ_r are computed as:

$$\varphi_m = B_r \cdot s_m L \quad , \quad \varphi_r = B_{sat} \cdot s_r L \qquad (18, 19)$$

where B_r is the PM remanence at the desired magnet temperature and $B_{sat} = 2.0$ T is the flux density of the saturated ribs.

The circuit is solved by applying the superposition principle: first the rotor flux generators are turned off and the flow-through (L_{fd}) component of L_{md} is evaluated. The remaining "circulating" component L_{cd} defined according to $L_{md} = L_{fd} + L_{cd}$ is calculated as in [7]. Second, the stator MMF generators to evaluate the PM flux linkage. The node-voltage analysis leads to the linear system:

$$\underbrace{\begin{bmatrix} \varphi_{b,k} - \varphi_{b,k+1} \\ \varphi_{b,k} - \varphi_{b,k+1} \\ \vdots \\ \varphi_{b,n} \end{bmatrix}}_{\boldsymbol{\Phi_b}} = \underbrace{\begin{bmatrix} \mathfrak{R}_{k,k}^{-1} & \mathfrak{R}_{k,k+1}^{-1} & \cdots & 0 \\ \mathfrak{R}_{k,k-1}^{-1} & \mathfrak{R}_{k,k}^{-1} & \cdots & 0 \\ \vdots & \vdots & \vdots & \vdots \\ 0 & 0 & \cdots & \mathfrak{R}_{n,n}^{-1} \end{bmatrix}}_{\mathfrak{R}^{-1}} \underbrace{\begin{bmatrix} r_1 \\ r_2 \\ \vdots \\ r_n \end{bmatrix}}_{\mathbf{r}} \quad (20)$$

$$\mathfrak{R}_{k,k}^{-1} = \mathfrak{R}_{b,k}^{-1} + \mathfrak{R}_{g,k}^{-1} + \mathfrak{R}_{b,k+1}^{-1} \qquad (21)$$

$$\mathfrak{R}_{k,k+1}^{-1} = -\mathfrak{R}_{b,k+1}^{-1} \qquad (22)$$

$$\mathfrak{R}_{k,k-1}^{-1} = -\mathfrak{R}_{b,k}^{-1} \qquad (23)$$

where $\mathbf{r}$ is the magnetic potential at the airgap (A point) and $\mathfrak{R}$ is the reluctance matrix. Note that k is the row index and the not-defined elements are null. Finally, the fundamental PM flux linkage is computed with the relationship (24)

$$\lambda_m = 2N_s k_w k_f \sum_{k=1}^{n} \frac{r_k}{\mathfrak{R}_{g,k}} \qquad (24)$$

where k_f stands for considering the fundamental harmonic only.

E. Radial ribs size

The size of the k-th radial rib is calculated as a function of (x, b) according to the material yield strength σ_y:

$$s_{r,rk} = \frac{m_j \cdot r_j \cdot n_{max}^2 \cdot (\pi/30)^2}{L \cdot \sigma_y} \qquad (25)$$

where m_j is the mass sustained by the j-th rib and r_j is the radial coordinate of its center of gravity. More details about this method are available in [17].

III. FEAfix REFINEMENT

The FEAfix refinement of the torque and PF versus (x, b) plane consists of a grid of FEA simulations on the design plane to fix the inaccuracies of the linear magnetic model. In this paper 16 simulations on a 4x4 grid in the plane are used. The simulated designs are marked with green dots in Fig. 6(a).

For each FEA-calculated design, the dq-flux linkage and current components in MTPA conditions are retrieved and used to correct the design equations. Two correction factors, one per axis, are defined as the ratio between the simulated and analytically computed flux linkage. The correction factors are extended to the (x, b) domain by linear interpolation. The approach is described in detail in [7]. For MTPA evaluation, each of the 16 FEAfix designs is evaluated at different γ angles at fixed current amplitude. Altogether, the torque and PF contours of the FEA-corrected design plane are the exact match of a fully-FEA evaluated response surface, obtained with a fraction of the computational time. To give a reference, the design plane of Fig. 6(a) was obtained in about 20 minutes using a PC with an Intel Xeon E5-2690 v4, 32GB RAM and 14 cores.

IV. CASE STUDY

The proposed design method is employed to design a motor after the Tesla Model 3 motor requirements of Tab. I. A double-V rotor is chosen, having the same number of pole pairs and slots of the Tesla benchmark, as well as the same slot fill factor, initial stack dimensions and power converter ratings. The flowchart of the design procedure is depicted in Fig. 5. Given the inputs, the design plane of Fig. 6(a) is obtained at a 36 A/mm^2, sustainable in a thermal short transient.

A. Torque and Power Factor Feasibility Area

The feasibility region of peak torque and power requirements is determined on the torque and PF plane of Fig. 6(a), by the intersection of the torque and PF target areas, highlighted in light green. Fig.6(b) reports the PM mass contours on the same plane, and the reference level 1.8 kg of the Tesla Model 3 benchmark. Most of the feasible designs exceed the PM mass limit. Yet, there is a small intersection between highlighted areas of Fig.6 (a) and (b), standing for designs with enough torque and power and less magnet.
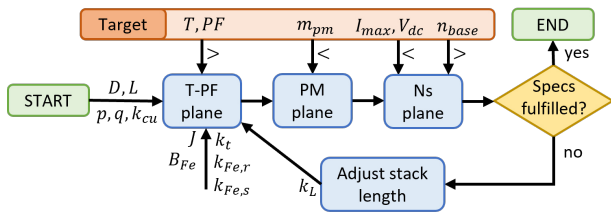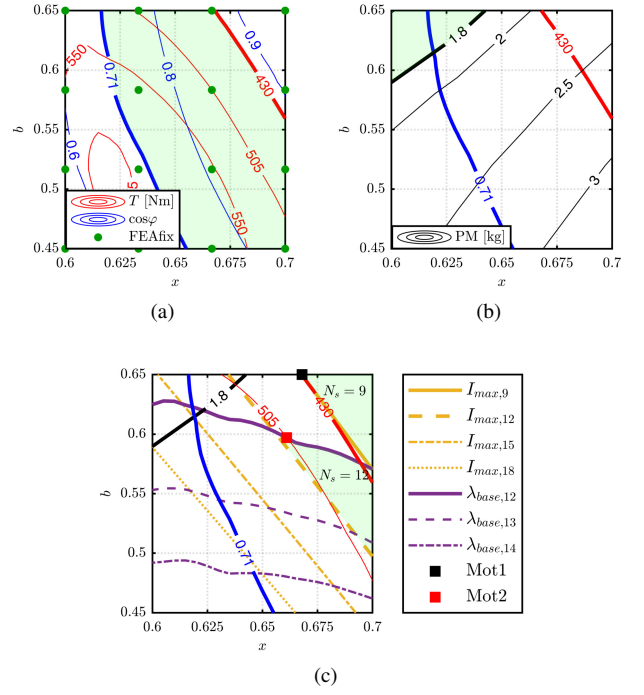

Fig. 5: Flowchart of the proposed design process.

Fig. 6: Design plane with full length: torque and PF contours (a) PM mass contours (b) I_{max,N_s} and λ_{max,N_s} contours (c).

B. Design of the Number of Turns

The number of turns N_s is selected to match the inverter voltage and current maximum ratings with the target base speed and peak torque. To address this task graphically, two novel contour types are displayed in Fig.6(c):

- I_{max,N_s} are the designs that have a phase current of I_{max} with N_s turns, given the current density and the torque specified by the design plane.
- λ_{base,N_s} are the designs that meet the specified base speed at the maximum inverter voltage with N_s turns.

The area above each I_{max,N_s} curve is where the torque and PF values prescribed by the plane are feasible with I_{max} or a lower current, provided that the machine has N_s turns in series. Similarly, the area below each λ_{base,N_s} contour is where the torque and PF prescribed by the plane are feasible with a voltage equal or lower than the DC-link limit, at the target base speed. For a given number of turns, the intersection of the two curves determines the designs that meet both the power converter requirements. Such areas must be crossed with the areas of feasibility of torque, PF and PM mass previously considered. Please note that feasible N_s values are multiple of 3 for this machine, which further limits the allowed solutions. Observing Fig. 6(c) the I_{max,N_s} and λ_{max,N_s} curves are considered for the feasible numbers $N_s = 9$ and $N_s = 12$.

C. Selection of Mot1

Mot1 (black square marker) in Fig. 6(c) is the only design that meets the magnetic specs (torque and PF) and

the converter specs (maximum current and voltage) with $N_s = 9$. However, being on the right side of the plane, the PM mass is 2 kg which is higher than the Tesla Model 3 target of 1.8 kg. Moreover, this design is at the torque border of the T-PF intersection area, which means that torque at maximum inverter current will be exactly 430 Nm with no margin, whereas the PF at base speed is much higher than the specified one (large margin).

D. Selection of Mot2

Mot2 (red square marker) is one feasible solution with $N_s = 12$, selected at the crossing between the $I_{max,12}$ and $\lambda_{base,12}$ contours, which also cross the 505 Nm contour in the same point. This means that this design is expected to have the desired base speed at maximum voltage and the displayed torque (505 Nm) at maximum inverter current, which is the target torque exceeded by $+17\%$. Finally, also Mot2 exceeds the PM mass limit, having a PMs mass of around 2.3 kg. In conclusion, both the selected designs match the peak torque and power output of the Tesla Model 3 benchmark in the same stack dimensions, with the same current density and the same power converters. However, both use a higher PM mass, and Mot2 in particular. Yet, Mot2 has redundant torque capability, which suggests that the stack length (and therefore PM mass) can be further optimized.

E. "Short" designs Mot2s and Mot3s

The stack length of Mot2 is reduced by a factor of $0.85 = \frac{430\,Nm}{505\,Nm}$, and the PM mass varies accordingly. The shortened Mot2s ("s" stands for "short") has a stack length of 114 mm and a PM mass of 1.93 kg. At the same time, the base speed increases inversely with the stack scaling factor, leading to exceed the base speed limit (4900 rpm vs 4200 rpm), with the same number of turns in series of 12. Thus, the shorter design Mot2s complies or exceeds the requirements of the Tesla Model 3 benchmark (same peak torque and higher peak power with a shorter stack), but yet with a higher PM mass.

For further optimization, the new design plane of Fig. 7 is launched, referring to the new stack length of 114 mm. All the other settings of the plane are unchanged (outer diameter, current density, geometric coefficients, ...). Please notice that:

- the torque contours of the new plane are obtained by scaling the ones of the previous plane by 0.85 times. This intuitively shrinks the corresponding area of feasibility in Fig. 7(a);
- the PF contours are unchanged;
- the PM mass contours shift down, enlarging the area of feasibility in Fig. 7(b);
- the I_{max,N_s} contours are unchanged;
- the λ_{base,N_s} contours shift upwards in proportion to the length scaling, thus enlarging the area of feasibility of the corresponding number of turns, as visible in Fig. 7(c);

The green square marker of Fig. 7(c) represents the latter design Mot2s, which belongs to the new design plane. The
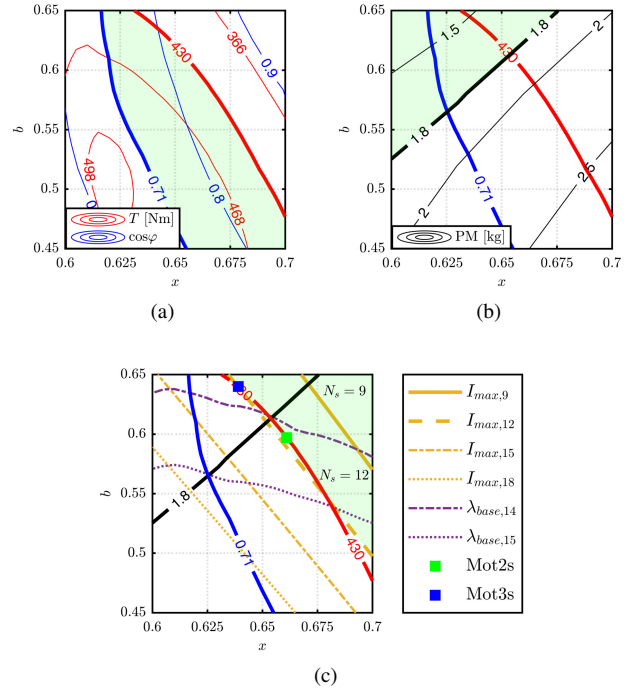

Fig. 7: Design plane with decreased length: torque and PF contours (a) PM mass contours (b) I_{max,N_s} and λ_{max,N_s} contours (c).

plane confirms that its peak torque matches the 430 Nm specification exactly, at the current limit. It also confirms that the PM mass is yet a slightly higher than the 1.8 kg target.

Intersecting the areas of feasibility of the three sub-figures, a region of PM mass minimization appears possible. The final machine Mot3s is chosen at the intersection between 430 Nm and $I_{max,12}$. The resulting design is expected to have the target torque with a shorter stack and lower PM mass, and exceeding base speed and hence exceeding peak power with respect to the benchmark case. The PF is higher but close to the minimum target. Lower iron and PM losses are also expected due to the volume reduction.

F. FEA Validation and Discussion

To complete the evaluation of the designed motors, their flux linkage and loss maps are FEA computed. The torque-speed limit curves are retrieved according to the said inverter limits, considering MTPA and maximum torque per voltage (MTPV) control strategies, as in [18], obtaining the Fig. 9.

The final figures of all the motors are reported in Table II for comparison with the benchmark, and their cross-sections are displayed in Fig. 9. Note that the cross-sections of Mot2 and Mot2s are the same, as said.

Dealing with full-length solutions Mot1 and Mot2, the first one overly exceeds the desired power in the flux-weakening speed range, whereas the second one exceeds the torque request. In both cases, the price to pay is the large PM quantity. Notably, Mot1 is not length-scalable not having torque margin at low speed. Mot2s loses some torque

TABLE II: Motor comparison, $V_{dc} = 231$ V, $I_{max} = 1414$ Apk, $\theta_{PM} = 80\,°C$

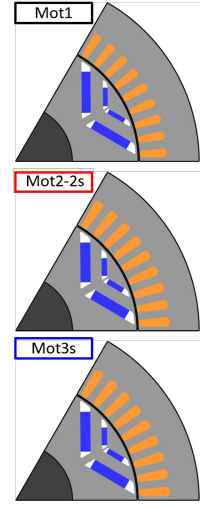|	Mot1	Mot2	Mot2s	Mot3s	Benchmark	
x	0.668	0.661	0.661	0.639	0.666	
b	0.650	0.597	0.597	0.640	0.596	
Max current density	36.2	37	37	36	36	[Apk/mm^2]
Max torque	430	518	441	430	430	[Nm]
Characteristics current	1366	1092	1092	928	1091	[A]
Base speed	5400	4200	4900	4800	4200	[rpm]
Max power	270	246	247	229	200	[kW]
Max power at max speed	270	220	223	190	163	[kW]
Turns	9	12	12	12	12	
Stack length	134	134	114	114	134	[mm]
PM mass	2.05	2.26	1.93	1.55	1.80	[kg]
Total stack mass	35.1	34.9	30.0	30.3	33.7	[kg]
Power density	7.7	7.1	8.2	7.6	5.9	[kW/kg]
Torque density	12.2	14.8	14.7	14.2	13.1	[Nm/kg]
Power per PM mass	132	109	128	147	111	[kW/kg]

Fig. 8: Motor sections.

Fig. 9: Torque (a) and power (b) versus speed of the designed motors at PMs temperature of 80 °C.
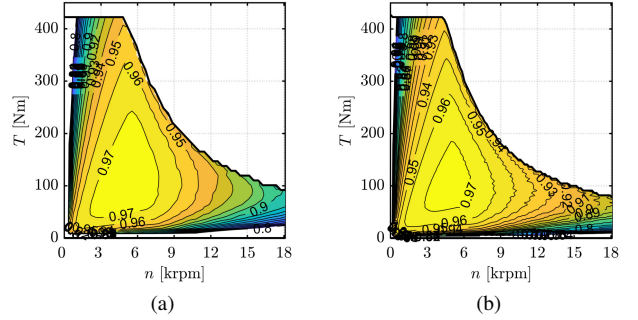

Fig. 10: Efficiency maps of Mot3s (a) and of the Tesla benchmark (b).

Fig. 11: Current limit corresponding to less than 1% of demagnetized PMs area vs PMs temperature.

with respect to Mot2, but has a very competitive power curve despite the reduced mass and PM mass. Finally, the PM-mass optimized solution Mot3s has the lowest power curve of the lot, but matches the benchmark output specs with a smaller stack volume and weight and with less PMs. Altogether, the short designs Mot2s and Mot3s are considered the best tradeoffs between cost, weight and performance. Dealing with loss and efficiency, the loss maps are evaluated as described in [18] and used to retrieve the efficiency maps. These are reported for Mot3s and for the Tesla benchmark only in Fig. 10. Please notice that the 0.97 sweet spot is larger for the smaller motor.

G. Demagnetization analysis

The steady-state demagnetization limit is evaluated by means of FEA simulations for all the considered machines. This consists of a sequence of fast FEA simulations where a current of growing amplitude is supplied against the PMs until the objective of 1% of demagnetized PM area is reached. For each current value, the flux density of each node of the PM mesh is extracted and the percentage PM volume below

the demagnetization limit is computed. The PM temperature θ_{PM} is also iterated in the analysis, leading to the results of Fig. 11. The analysis demonstrates that all the new designs are equal or better than the reference motor in term of steady-state demagnetization limit.

V. Conclusion

A fast and effective procedure for the preliminary design of IPM machines is presented. The method is presented with reference to traction application and the Tesla Model 3 front-axle IPM motor. Four preliminary designs are found in relatively short computational time, all fulfilling or exceeding the benchmark specifications in terms of output figures, weight and volume of the active parts and robustness to demagnetization. It is exhibited how the procedure can aid the designers detecting feasible and optimal solutions, and how to minimize the axial dimension and the PM mass. The results of the paper are intended for showcasing the potential and prospects of the new design method, which is meant as a powerful starting point for more meticulous and time consuming thermal and mechanical optimization.

VI. Akcnowledgments

References

[1] A. Krings and C. Monissen, "Review and Trends in Electric Traction Motors for Battery Electric and Hybrid Vehicles," in *2020 International Conference on Electrical Machines (ICEM)*, 2020, pp. 1807–1813.

[2] W. Cao, B. C. Mecrow, G. J. Atkinson, J. W. Bennett, and D. J. Atkinson, "Overview of Electric Motor Technologies Used for More Electric Aircraft (MEA)," *IEEE Transactions on Industrial Electronics*, vol. 59, no. 9, pp. 3523–3531, Sep. 2012.

[3] J. Benzaquen, J. He, and B. Mirafzal, "Toward more electric powertrains in aircraft: Technical challenges and advancements," *CES Transactions on Electrical Machines and Systems*, vol. 5, no. 3, pp. 177–193, Sep. 2021.

[4] V. Yaramasu, B. Wu, P. C. Sen, S. Kouro, and M. Narimani, "High-power wind energy conversion systems: State-of-the-art and emerging technologies," *Proceedings of the IEEE*, pp. 740–788, May 2015.

[5] A. Binder and T. Schneider, "Permanent magnet synchronous generators for regenerative energy conversion - a survey," in *2005 European Conference on Power Electronics and Applications*, Sep. 2005.

[6] Z. Q. Zhu, W. Q. Chu, and Y. Guan, "Quantitative comparison of electromagnetic performance of electrical machines for HEVs/EVs," *CES Transactions on Electrical Machines and Systems*, vol. 1, no. 1, pp. 37–47, Mar. 2017.

[7] S. Ferrari and G. Pellegrino, "FEAfix: FEA Refinement of Design Equations for Synchronous Reluctance Machines," *IEEE Transactions on Industry Applications*, vol. 56, no. 1, pp. 256–266, Jan. 2020.

[8] B. Boazzo, A. Vagati, G. Pellegrino, E. Armando, and P. Guglielmi, "Multipolar Ferrite-Assisted Synchronous Reluctance Machines: A General Design Approach," *IEEE Transactions on Industrial Electronics*, vol. 62, no. 2, pp. 832–845, Feb. 2015.

[9] N. Rivière, M. Stokmaier, and J. Goss, "An Innovative Multi-Objective optimization Approach for the Multiphysics Design of Electrical Machines," in *2020 IEEE Transportation Electrification Conference Expo (ITEC)*, Jun. 2020, pp. 691–696, iSSN: 2377-5483.

[10] G. Lei, J. Zhu, Y. Guo, C. Liu, and B. Ma, "A Review of Design Optimization Methods for Electrical Machines," *Energies*, vol. 10, no. 12, p. 1962, Dec. 2017.

[11] K.-C. Kim, J. Lee, H. J. Kim, and D.-H. Koo, "Multiobjective Optimal Design for Interior Permanent Magnet Synchronous Motor," *IEEE Transactions on Magnetics*, vol. 45, no. 3, pp. 1780–1783, Mar. 2009.

[12] P. Ragazzo, S. Ferrari, N. Riviere, M. Popescu, and G. Pellegrino, "Efficient Multiphysics Design Workflow of Synchronous Reluctance Motors," in *2020 International Conference on Electrical Machines (ICEM)*. Gothenburg, Sweden: IEEE, Aug. 2020, pp. 2507–2513. [Online]. Available: https://ieeexplore.ieee.org/document/9270670/

[13] M. Barcaro, G. Meneghetti, and N. Bianchi, "Structural analysis of the interior pm rotor considering both static and fatigue loading," *IEEE Transactions on Industry Applications*, vol. 50, pp. 253–260, 2014.

[14] MotorXP, *Performance Analysis of the Tesla Model 3 Electric Motor using MotorXP-PM*. VEPCO, Jun. 2020. [Online]. Available: https://motorxp.com/wp-content/uploads/mxp_analysis_TeslaModel3.pdf

[15] F. Cupertino and G. Pellegrino, "SyR-e: Synchronous Reluctance (machines) - evolution." [Online]. Available: www.github.com/SyR-e

[16] T. A. Lipo, *Introduction to AC Machine Design*, Hoboken, NJ, USA: Wiley, 2017.

[17] F. Cupertino, M. Palmieri, and G. Pellegrino, "Design of high-speed synchronous reluctance machines," in *2015 IEEE Energy Conversion Congress and Exposition (ECCE)*, Sep. 2015, pp. 4828–4834, iSSN: 2329-3748.

[18] S. Ferrari, P. Ragazzo, G. Dilevrano, and G. Pellegrino, "Flux-Map Based FEA Evaluation of Synchronous Machine Efficiency Maps," in *2021 IEEE Workshop on Electrical Machines Design, Control and Diagnosis (WEMDCD)*, Apr. 2021, pp. 76–81.

VII. Biographies

Paolo Ragazzo (S'20) is currently pursuing the Ph.D. degree at Politecnico di Torino, Turin, Italy. He received the B.S. and M.Sc. degrees in Electrical Engineering from Politecnico di Torino in 2017 and 2020, respectively. He was an Exchange Student at the Norwegian University of Science and Technology (NTNU), Trondheim, Norway and an Intern at Motor Design Ltd, Wrexham, United Kingdom. His research activity relates to electric traction motors with emphasis on performance estimation and multiphysics modelling.

Gaetano Dilevrano (S'20) received the B.Sc. and M.Sc degrees in Electrical Engineering from Politecnico di Torino, Turin, Italy in 2017 and 2020, respectively. He is currently a Ph.D. student in Electrical, Electronics, and Communications Engineering at Politecnico di Torino. His research activity relates to the design and test procedures of electric motors and drives for electric and hybrid vehicle powertrains with emphasis on innovative electric machines, integration of machine and power converter and advanced test methodologies.

Simone Ferrari (S'17-M'20) received the Ph.D. degree "cum laude" in 2020 from Politecnico di Torino, Turin, Italy, where he is currently a Research Fellow. From July to December 2018, he was a Visiting Scholar with North Carolina State University, Raleigh, NC, USA. He is one of the authors of SyR-e, an open-source design tool for synchronous reluctance and permanent magnet machines. His research interests include electrical machine design and multiphysical evaluation of electrical machines, with a focus on synchronous reluctance and permanent magnet machines.

Gianmario Pellegrino (M'06–SM'13-F'22) received the M.Sc. and Ph.D. degrees in electrical engineering from Politecnico di Torino, Turin, Italy, in 1998 and 2002, respectively. He is currently a Professor of power converters, electrical machines and drives with Politecnico di Torino. He was a Visiting Fellow with Aalborg University, Denmark, the University of Nottingham, U.K., and the University of Wisconsin, Madison, USA. He is one of the authors of the open, source project SyRe for the design of electrical motors and three patents. He is engaged in several research projects with the industry. Dr. Pellegrino is an Associate Editor for the IEEE Transactions on Industry Applications. He was the recipient of more than 55 IEEE journal papers and nine Best Paper Awards. He is a member of the Power Electronics Interdepartmental Laboratory (PEIC) established in 2017 at the Politecnico di Torino and a member of the Advisory Board of PCIM (Power Conversion and Intelligent Motion) Europe. He is currently the Rector's Advisor for Interdepartmental Centres, Politecnico di Torino.